https://doi.org/10.5194/egusphere-2023-2196
Preprint. Discussion started: 13 October 2023
© Author(s) 2023. CC BY 4.0 License.

Moist bias in the Pacific upper troposphere and lower stratosphere (UTLS) in climate models affects regional circulation patterns

Felix Ploeger[1,2], Thomas Birner[3], Edward Charlesworth[1], Paul Konopka[1], and Rolf Müller[1]

[1]Institute for Energy and Climate Research: Stratosphere (IEK–7), Forschungszentrum Jülich, Jülich, Germany.
[2]Institute for Atmospheric and Environmental Research, University of Wuppertal, Wuppertal, Germany.
[3]Meteorological Institute Munich, Ludwig Maximilians University of Munich, Munich, Germany.

Correspondence: Felix Ploeger (f.ploeger@fz-juelich.de)

Abstract. Water vapour in the UTLS is a key radiative agent and crucial factor in the Earth's climate system. But global climate models face problems with simulating the largest UTLS moisture anomaly in the boreal summertime Asian monsoon region and simulate a common regional moist bias in the Pacific UTLS. We demonstrate from combination of climate model experiments and atmospheric observations that the Pacific moist bias critically impacts regional circulation systems by inducing local longwave cooling. Related impacts involve a strengthening of isentropic potential vorticity gradients, strengthened westerlies in the Pacific westerly duct region, and a zonally extended anticyclonic monsoon circulation. We further show that the regional Pacific moist bias can be significantly reduced by applying a Lagrangian, less diffusive transport scheme and that such model improvement could be an important factor for improving simulation of regional circulation systems, in particular in the Asian monsoon and Pacific region.

1 Introduction

Notwithstanding the low abundance of water vapour in the stratosphere, with mixing ratios on the order of parts per million beyond the cold tropical tropopause (Brewer, 1949; Fueglistaler et al., 2005), stratospheric water vapour variations play a crucial role for climate variability. Variations in stratospheric water vapour have been shown to modify past global warming by up to 30% (Solomon et al., 2010). In a future climate with rising greenhouse gas levels, climate models predict significant stratospheric water vapour increases, strongest in the lowermost stratosphere directly above the extratropical tropopause (Dessler et al., 2013; Banerjee et al., 2019). The processes causing this increase are under debate (Dessler et al., 2016; Smith et al., 2022; Hoor et al., 2010). Recently, indications for a positive trend in water vapour in the stratosphere have also been found from satellite observations (Konopka et al., 2022). As stratospheric water vapour acts as an impactful greenhouse gas, an increase in its abundance will cause a positive climate feedback of about 0.1-0.26 $Wm^{-2}K^{-1}$ (Banerjee et al., 2019) and substantial effects on atmospheric temperatures and dynamics (Li and Newman, 2020), with the largest fraction of these effects caused by water vapour increases in the lowermost stratosphere.

However, it is particularly the lowermost stratosphere where current global climate models show the largest biases between simulations and observations in stratospheric water vapour (Keeble et al., 2021). These moist biases in the simulations in the lowermost stratosphere appear to be related to numerical diffusion in model transport schemes and can be significantly reduced

https://doi.org/10.5194/egusphere-2023-2196
Preprint. Discussion started: 13 October 2023
© Author(s) 2023. CC BY 4.0 License.

when employing less diffusive Lagrangian schemes (Stenke et al., 2009; Charlesworth et al., 2023). Charlesworth et al. (2023) showed that lower stratospheric water vapour exerts a first order effect on zonal mean atmospheric circulation, with water vapour increases (e.g. the model moist bias) causing a strengthening of the stratospheric circulation, upward and poleward shifts of the subtropical jets, and a poleward shift of the tropospheric eddy-driven jet. Hence, improving the representation of stratospheric water vapour in climate models appears to be essential for improving the simulation of zonal mean circulation in climate models and future projections.

A particularly strong moisture source for the lower stratosphere is the anticyclonic Asian monsoon circulation during boreal summer (Randel and Park, 2006; Garny and Randel, 2013), which causes the ascending moist air masses to partly bypass the coldest regions of the tropical tropopause and to retain relatively high moisture (James et al., 2008; Wright et al., 2011; Nützel et al., 2019). Although the air masses are, to some degree, confined within the monsoon anticyclone (Park et al., 2009; von Hobe et al., 2021; Legras and Bucci, 2020), Rossby-wave breaking along the anticyclone edge may cause substantial transport of moisture into the extratropical lowermost stratosphere (Ploeger et al., 2013; Rolf et al., 2018). Analysis of the distribution of water vapour in the lower stratosphere simulated by a climate model has shown a substantial model bias in the Asian monsoon region (Wang et al., 2018). In the model, the maximum moisture anomaly was found to be displaced far into the Pacific region, as compared to satellite observations which show the moisture maximum in the Asian monsoon circulation. Wang et al. (2018) further showed that this model bias was likely a transport issue and could be reduced by increasing the model resolution.

Here, we combine a dedicated climate model experiment with the ECHAM MESSy Atmospheric Chemistry model (EMAC), statistical analysis of a suite of historical climate model simulations from the Coupled Model Intercomparison Project (CMIP6), and satellite observations by the Microwave Limb Sounder (MLS) to investigate regional water vapour anomalies in the UTLS and related effects on regional circulation systems. The EMAC model experiment employs either the standard "control" configuration or a new "modified–Lagrangian" transport scheme with the Chemical Lagrangian Model of the Stratosphere (CLaMS) coupled to EMAC (Methods), allowing the effects of model transport on stratospheric water vapour to be isolated. These EMAC model simulations are the same as those recently published by Charlesworth et al. (2023), but here we extend their zonal mean analysis to a regional level to address the following questions: (i) Where are the strongest regional biases in UTLS water vapour in current climate models? (ii) How do regional anomalies in UTLS water vapour affect regional atmospheric circulation systems, in particular in the Asian monsoon and in the Pacific region?

2 Results

The strongest regional water vapour anomalies in the UTLS occur in the Asian and North American monsoon circulations (Schoeberl et al., 2013), with the relative strength between Asian and American anomalies under debate (Plaza et al., 2021). At 100 hPa, a common level for studying UTLS water vapour, satellite observations by MLS (Methods) show almost 2 ppmv (around 40%) higher water vapour mixing ratios above Asia than above the Pacific during boreal summer (Fig. 1a). Current global climate models from the CMIP6 model intercomparison project also show largest regional water vapour biases in that region (Fig. 1b), and a substantial displacement of the moisture anomaly towards the Pacific when compared to satellite

https://doi.org/10.5194/egusphere-2023-2196
Preprint. Discussion started: 13 October 2023
© Author(s) 2023. CC BY 4.0 License.

observations. This moisture bias has already been reported by Wang et al. (2018) and has been related to transport effects, but only for a single model. Here, we show that in the Pacific UTLS the moisture bias is a common feature of the CMIP6 models, clearly visible in the multi-model mean (Fig. 1b), and reaching even higher values for specific models (Supplement Fig. S3 and S4).

Consistent with the CMIP6 models, also the EMAC climate model in its control set-up (Methods) shows a strong moisture bias in the summertime UTLS above the Pacific (Fig. 1d). In EMAC, the moist bias extends even further across the Pacific than for the CMIP6 multi-model mean. After switching to a Lagrangian transport scheme, the modified–Lagrangian EMAC–CLaMS simulation (Methods) shows remarkably better agreement with MLS satellite observations in terms of UTLS water vapour (Fig. 1c). Hence, Lagrangian transport appears to avoid the strong regional moisture bias in the summertime Pacific lower stratosphere in current global climate model simulations. Note, that the global mean water vapour mixing ratio in the modified–Lagrangian simulation is too low compared to MLS observations, due to a known cold bias in TTL temperatures in EMAC, but the focus of the present paper is on regional anomalies.

Water vapour is a radiatively active gas, thus the enhanced moisture above the Pacific in the control EMAC model simulation affects atmospheric temperatures and circulation. The enhanced moisture causes longwave cooling which decreases temperatures in the UTLS above the Pacific (Fig. 1d, white contours). These decreased temperatures imply increased westerly zonal wind and decreased (more equatorward) meridional wind above the Pacific, consistent with thermal wind balance (Methods). Consistently, potential vorticity (PV) increases, the horizontal PV gradient strengthens, and the westerlies in the Pacific UTLS close to the equator amplify (Fig. 1d, see also Discussion) in response to the enhanced moisture in the Pacific UTLS.

Latitude-altitude cross-sections in the Pacific UTLS (Fig. 2a–c) show that the enhanced moisture in the control EMAC simulation extends well above the tropopause, causing enhanced longwave cooling (cyan contours) and decreased temperatures particularly in the lowermost stratosphere. As discussed above, related to the enhanced moisture is also a strengthened isentropic PV gradient, with pronounced strengthening around the tropopause (Fig. 2d–f). Notably, the water vapour contours in the control EMAC simulation are not following the PV structure, indicating a decoupling of the simulated water vapour distribution from large-scale transport processes. Satellite observations, on the other hand, show a clear anticorrelation between water vapour mixing ratios and PV in the UTLS (correlation coefficient -0.62, slope -0.53), which is opposite in the control EMAC simulation (positive correlation 0.78 and slope 1.24, see Fig. 2g, h). Again, the modified–Lagrangian simulation avoids this transport bias and results in much better agreement with the observations (correlation coefficient -0.86, slope -0.53, Fig. 2i).

The unphysical correlation between water vapour mixing ratios and PV is an indication that the moisture bias in the control simulation is caused by small-scale, unresolved processes, namely numerical diffusion in the advective transport scheme (see Charlesworth et al., 2023, and Methods). The less diffusive Lagrangian transport scheme in the modified–Lagrangian EMAC–CLaMS model results in a more efficient sampling of cold tropopause regions and in less moisture transport into the lower stratosphere. Indeed, it is just the change in the model transport scheme and not the induced circulation changes which reduces the moist bias, as a sensitivity simulation without including the dynamical feedback of the water vapour changes provided very similar results to the modified–Lagrangian simulation with dynamical feedback included (see Supplement Fig. S1).

https://doi.org/10.5194/egusphere-2023-2196
Preprint. Discussion started: 13 October 2023
© Author(s) 2023. CC BY 4.0 License.

Moreover, the enhanced Pacific moisture exerts an effect on the Asian monsoon circulation, which is located to the west of the moisture enhancement. Differences in meridional velocity v between the control and the modified–Lagrangian simulations (Fig. 3a) show a strengthening of the equatorward flow on the eastern edge of the monsoon anticyclone related to the water vapour induced longwave cooling, decreased temperatures and modified zonal temperature gradient $\mathrm{d}T/\mathrm{d}x$ above the Pacific (Methods). Thus, the enhanced water vapour above the Pacific in control EMAC causes a strengthened, eastward shifted equatorward flow at the eastern edge of the monsoon anticyclone, resulting in a zonal broadening of the monsoon circulation.

Eastward of the Asian monsoon circulation is the region of the Pacific westerly ducts (Webster and Holton, 1982), where westerly winds may extend to and across the equator (Fig. 1e, f, yellow contours). These equatorial westerlies are strongest during boreal winter and the term "westerly ducts" had originally been introduced only for that season, but we use it here also for the boreal summer circulation. Differences between the control simulation and the modified–Lagrangian simulation of zonal u–wind in the subtropics (Fig. 3b) show that the westerlies above the Pacific (east of 140°E) strengthen in response to enhanced Pacific moisture, consistent with the water vapour–induced cooling and modified meridional temperature gradient $\mathrm{d}T/\mathrm{d}y$ (Methods). Thus, the moist bias in the Pacific UTLS is related to strengthened westerly ducts in the northern tropics and subtropics.

3 Discussion

As the Pacific UTLS moisture bias is similar between control EMAC and CMIP6 models, also effects on regional circulation systems are expected to be similar. In the CMIP6 models, the anticyclonic Asian monsoon circulation appears too strong and displaced towards the East when compared to ERA5 geopotential height (Fig. 4a, b), in particular when considering zonal geopotential height anomaly profiles across the anticyclone center (Fig. 4c, Methods). All CMIP6 models have a larger geopotential height anomaly on the eastern monsoon edge than ERA5, even outside the ERA5 year-to-year variability range (Fig. 4c, red error bars).

The CMIP6 inter-model correlation between local meridional v–wind velocity in the monsoon anticyclone and a water vapour index measuring the strength of the Pacific moisture anomaly (Methods) shows a significant anticorrelation eastward of 100°E (Fig. 3d). In other words, those models with a moister lower stratosphere above the Pacific simulate an anticyclonic monsoon circulation which extends further east. Likewise, the northward flow at the western edge of the monsoon anticylone increases and extends further west with increased Pacific water vapour across CMIP6 models (positive correlation westward of 60°E). Above the tropopause, this correlation pattern closely resembles the pattern of differences in meridional flow (v–wind) between the control and modified–Lagrangian simulations in the EMAC model experiment (Fig. 3a). Hence, the enhanced equatorward flow at the eastern monsoon anticyclone edge and enhanced poleward flow at the western edge appear related to the strength of the water vapour anomaly above the Pacific, in both the EMAC model experiment and in CMIP6 models. Those models with a moister Pacific UTLS simulate a zonally broader and stronger monsoon anticyclone.

Prevailing westerlies in the Pacific UTLS, the westerly ducts, allow Rossby waves to propagate further towards, even across the equator (Waugh and Polvani, 2000), and to cause inter-hemispheric exchange (Yan et al., 2021). Therefore, a realistic

https://doi.org/10.5194/egusphere-2023-2196
Preprint. Discussion started: 13 October 2023
© Author(s) 2023. CC BY 4.0 License.

representation of the westerly ducts in atmospheric models is important for correctly simulating the global distribution of trace gases and pollutants, especially for species with strong emissions in the Northern hemisphere. Zonal profiles of zonal wind in the northern tropics show that most CMIP6 models simulate too strong westerlies above the Pacific (Fig. 4d) compared to ERA5. Furthermore, CMIP6 inter-model correlations between zonal wind and Pacific UTLS moisture show a significant correlation in the Pacific subtropics around the tropopause (Fig. 3d). This correlation implies that those models with increased Pacific moisture simulate stronger westerly ducts, consistent with the effect of enhanced Pacific moisture in the EMAC model experiment (Fig. 3b). Hence, the overestimated westerly ducts in CMIP6 models appear to be related, at least partly, to the model moist bias above the Pacific.

4 Conclusions

We show that a distinct water vapour enhancement above the Pacific in the summertime UTLS is a common feature in current climate models. This regional moist bias is not related to large-scale transport characteristics and the expected anti-correlation between UTLS water vapour and PV breaks down. Furthermore, the bias can be significantly reduced by applying a Lagrangian, numerically less diffusive transport scheme, as realized in the modified–Lagrangian EMAC–CLaMS simulation. The analysis of a dedicated climate model experiment and CMIP6 models further shows that the Pacific moist bias affects regional circulation patterns by inducing local longwave cooling and modifying temperature gradients. In particular, our results indicate that the water vapour anomaly in the Pacific UTLS strengthens the Pacific westerly ducts and causes zonal broadening and amplification of the Asian monsoon upper level anticyclonic flow. Hence, improving the representation of water vapour in the Pacific UTLS region in models, for instance by employing less diffusive (e.g. Lagrangian) transport schemes, will affect regional circulation systems and could be a promising way to improve model simulations and predictability, for instance in the Asian monsoon and Pacific regions.

https://doi.org/10.5194/egusphere-2023-2196
Preprint. Discussion started: 13 October 2023
© Author(s) 2023. CC BY 4.0 License.

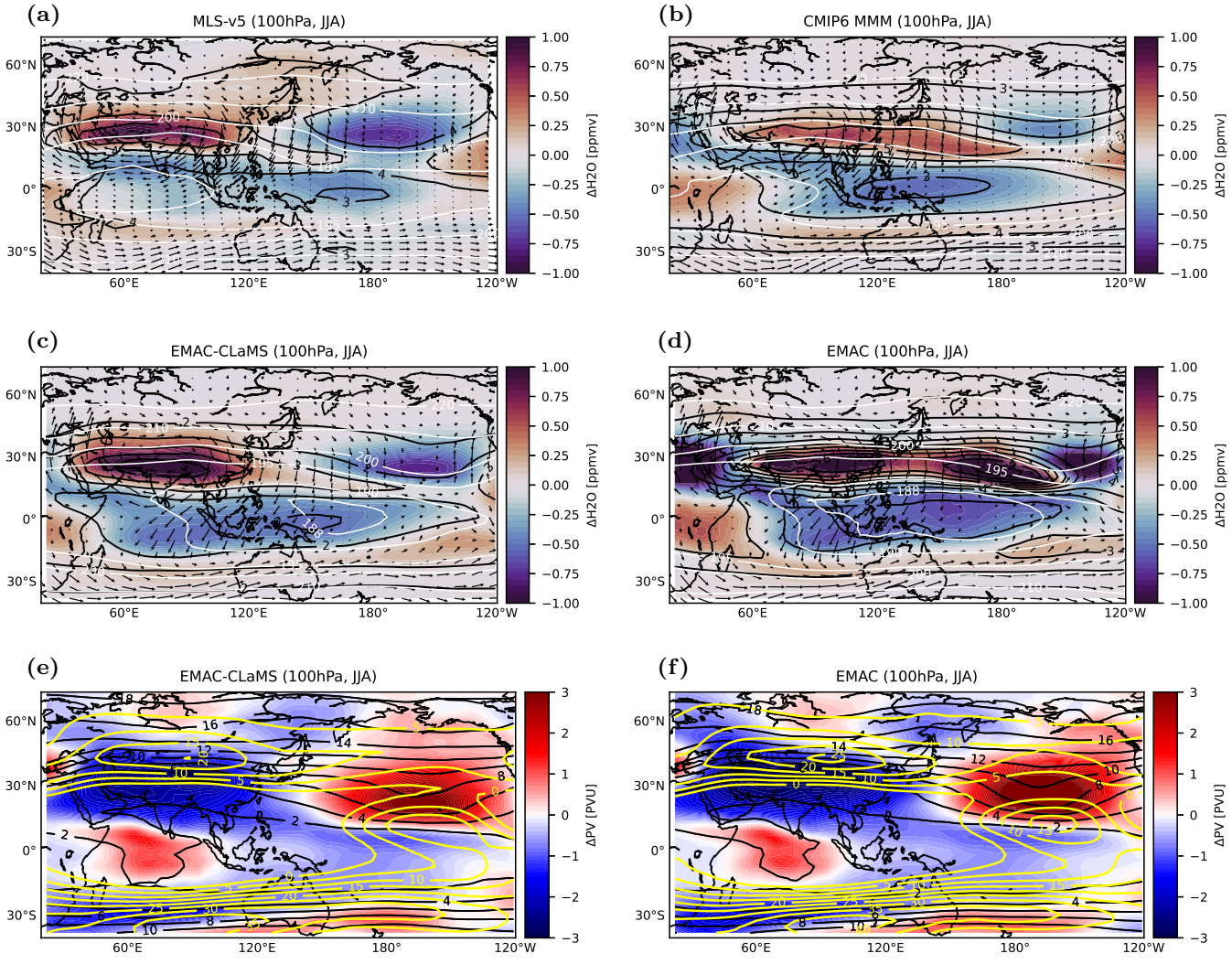

Figure 1. Water vapour zonal anomalies at 100 hPa in boreal summer (June–August) from (a) MLS–v5 and (b) CMIP6 multi-model mean, (c) modified–Lagrangian EMAC–CLaMS and (d) EMAC. Black contours show climatological water vapour mixing ratios, white contours temperature and black arrows the horizontal wind. (e–f) PV zonal anomalies at 100 hPa from EMAC–CLaMS (left) and EMAC (right), together with the climatological PV distribution (black contours, 2 PVU steps) and zonal wind distribution (yellow contours, 5 ms^{-1} steps for westerlies).

https://doi.org/10.5194/egusphere-2023-2196
Preprint. Discussion started: 13 October 2023
© Author(s) 2023. CC BY 4.0 License.

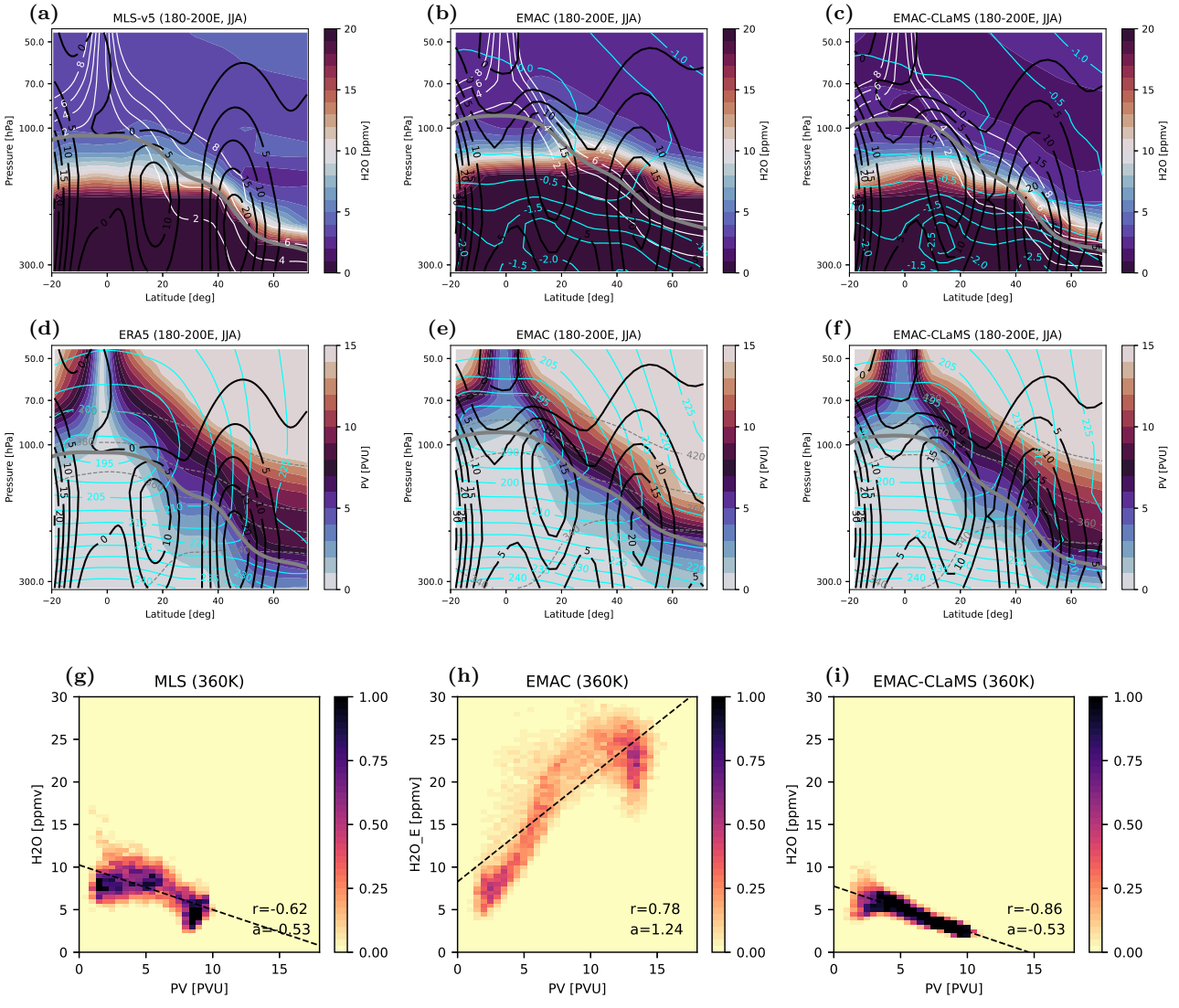

Figure 2. Water vapour cross-sections for the Pacific region (180°-200°E, bottom) in boreal summer (June–August), for (a) MLS satellite observations, (b) control EMAC, and (c) modified–Lagrangian EMAC–CLaMS simulations. Black thick contours show westerly zonal wind, thin white contours PV, cyan contours longwave radiative heating rate (in K/day), and the thick gray line the WMO lapse rate tropopause. PV sections in the same region are shown for (d) ERA5, (e) EMAC, and (f) Lagrangian EMAC–CLaMS, together with westerly zonal wind (black contours), temperature contours (cyan) and potential temperature (gray dashed lines, 340, 360, 380, 420 K). Correlation between water vapour and potential vorticity at 360 K potential temperature level in the Pacific region (15°-70°N, 140°-240°E) for (g) MLS satellite observations and ERA5 reanalysis PV, (h) control EMAC, and (i) modified–Lagrangian EMAC–CLaMS. The Pearson correlation coefficient r and linear regression slope a are given in each figure and the linear regression fit is illustrated as black dashed line.

https://doi.org/10.5194/egusphere-2023-2196
Preprint. Discussion started: 13 October 2023
© Author(s) 2023. CC BY 4.0 License.

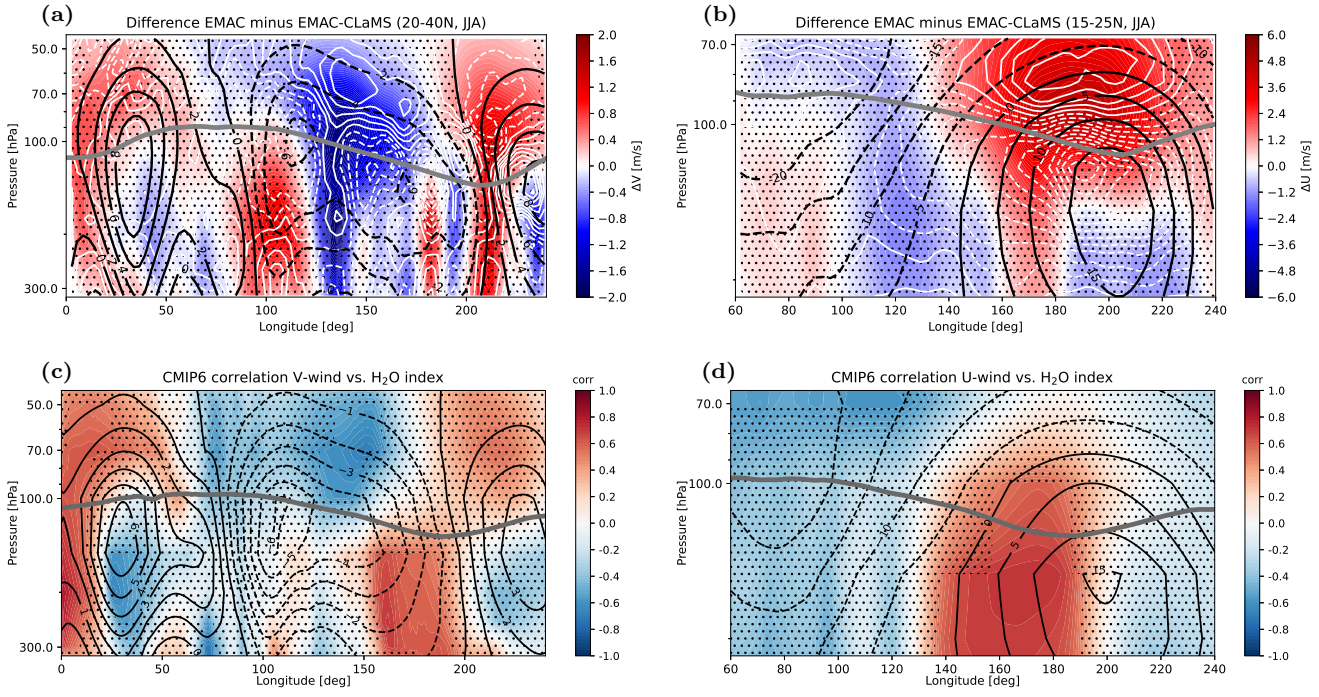

Figure 3. (a) Difference in meridional v–wind between control EMAC minus modified–Lagrangian EMAC–CLaMS for a longitude section across the Asian monsoon ($20^\circ - 30^\circ$N) for boreal summer (June–August). White contours show the model difference for the zonal temperature gradient $\mathrm{d}T/\mathrm{d}x$, black contours show climatological meridional wind values (from modified–Lagrangian simulation), the thick grey line is the tropopause. Black dots indicate where the difference is not statistically significant at 95% confidence level. (b) Same model difference (control minus modified–Lagrangian), but for zonal u–wind and as longitude profile in the subtropics ($15^\circ - 25^\circ$N). White contours show the model difference for the meridional temperature gradient $\mathrm{d}T/\mathrm{d}y$, black contours show climatological zonal wind values (from modified–Lagrangian simulation), the thick grey line is the tropopause. (c) The CMIP6 inter-model correlation between meridional v–wind and the Pacific H_2O index measuring the strength of the Pacific moisture anomaly in the different models (see Methods for details). Solid black lines show multi-model mean zonal wind, the grey line the tropopause from ERA5. Black dots indicate where the correlation is not significant at 95% confidence level. (d) CMIP6 inter-model correlation between zonal wind and the Pacific H_2O index. Solid black lines show multi-model mean zonal wind, the grey line the tropopause from ERA5.

https://doi.org/10.5194/egusphere-2023-2196
Preprint. Discussion started: 13 October 2023
© Author(s) 2023. CC BY 4.0 License.

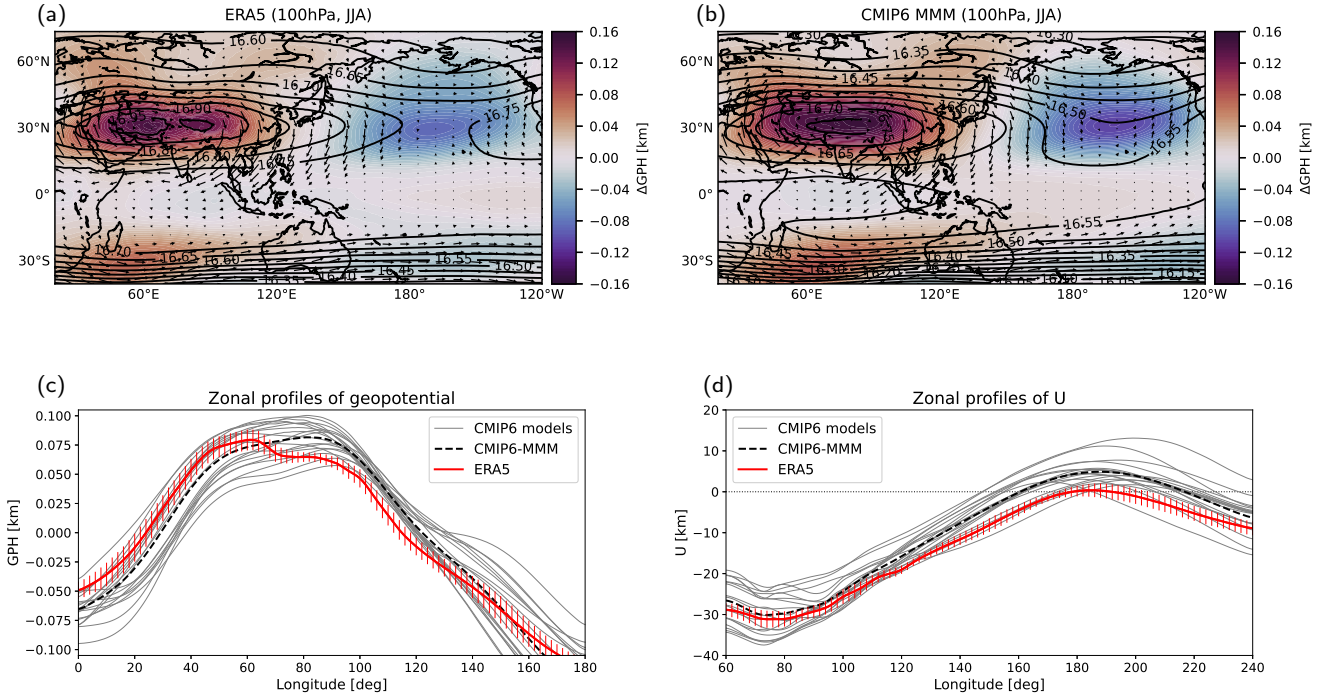

Figure 4. Geopotential height zonal anomalies at 100 hPa for boreal summer (June–August), from (a) ERA5 and (b) CMIP6 multi-model mean. Black contours show climatological geopotential height and black arrows the horizontal wind. (c) Zonal profiles of geopotential height at the latitude of the monsoon geopotential height maximum (Methods), from CMIP6 models (grey), multi-model mean (black) and ERA5 (red). Red error bars show the standard deviation of year-to-year variability for ERA5 data. (d) Zonal profiles of zonal wind at 15°N from CMIP6 models (grey), multi-model mean (black) and ERA5 (red).

https://doi.org/10.5194/egusphere-2023-2196
Preprint. Discussion started: 13 October 2023
© Author(s) 2023. CC BY 4.0 License.

5 Appendix

5.1 Methods

5.1.1 Satellite observations

The simulated water vapour distributions from the different models are compared to observations from the Microwave Limb Sounder (MLS) instrument onboard the Aura satellite (version 5 data), which has started operation in 2004. MLS provides a relatively high sampling of the globe from about 82°S-82°N, with about 3500 profiles per day. In the UTLS region, the MLS water vapour product has a vertical resolution of about 3 km. The MLS averaging kernels have been shown to induce artifacts in the water vapour distribution, in particular vertical oscillations at high latitudes (Ploeger et al., 2013), but have no large influence on lower, subtropical latitudes, which are the focus of this paper. As the main goal of the paper is to investigate differences between model simulations, we refrain from smoothing the model profiles with the satellite averaging kernels. For comparison with the model data, monthly mean climatologies have been compiled from the MLS data on the original MLS pressure levels and for the period 2005–2015. For further information on MLS water vapour and the retrieval technique see Read et al. (2007).

5.1.2 EMAC model simulations

The chemistry climate model used for this study is the ECHAM/MESSy Atmospheric Chemistry model (EMAC). EMAC couples the ECHAM5 dynamical core to physical processes via the Modular Earth Submodel System (MESSy) middleware (for details see Jöckel et al., 2016, and references therein). The simulations analyzed for this study employ a T42 spectral resolution (about 2.8×2.8 degrees latitude-longitude resolution), 90 vertical levels from the surface to 0.01 hPa, and are free-running with prescribed sea surface temperatures and radiatively active substances (for further details see Charlesworth et al., 2023). The simulation period spans 40 years starting 1970, with only the last ten years (2000–2009) considered for this paper.

Water vapour is calculated online and includes methane oxydation as chemical source in the stratosphere. In particular, we compare two different simulations with stratospheric water vapour transported either with the Flux-Form Semi-Lagrangian standard EMAC transport scheme (denoted “control” EMAC) or with the Lagrangian transport scheme CLaMS (Chemical Lagrangian Model of the Stratosphere), denoted “modified–Lagrangian” EMAC, as described by Charlesworth et al. (2023). Due to its Lagrangian nature, the CLaMS transport scheme has largely reduced numerical diffusion compared to the standard EMAC transport (Hoppe et al., 2014; Charlesworth et al., 2020). In both simulations the water vapour is coupled to the model radiation and thereby affects atmospheric temperature and circulation. Note that the Lagrangian water vapour calculation for this study only ranges from about 250 hPa to the model top, to ensure that model differences originate solely from stratospheric water vapour. As the only difference between both simulations is the used transport scheme for stratospheric water vapour, differences in temperatures and circulation can be unambiguously attributed to the transport scheme.

To further clarify the roles of the changed transport scheme versus the induced dynamical effects for the water vapour model differences, an additional sensitivity simulation was carried out with stratospheric water vapour calculated with Lagrangian

https://doi.org/10.5194/egusphere-2023-2196
Preprint. Discussion started: 13 October 2023
© Author(s) 2023. CC BY 4.0 License.

CLaMS transport but not coupled to radiation. The close similarity of the lower stratospheric water vapour distribution with the modified Lagrangian simulation (with stratospheric water vapour coupled to radiation) shows that the water vapour differences compared to the control EMAC simulation are mainly related to the difference in the transport scheme (numerical diffusion) and not to the induced dynamical effects (Supplement Fig. S1).

A second sensitivity simulation was carried out for the first year of the simulation period with tendency output for the control EMAC water vapour. These additional diagnostic terms which are output by EMAC include the tendencies due to advection, clouds (mainly dehydration processes at levels around the tropopause), convection, and parameterized vertical diffusion (Supplement Fig. S2). Consideration of the different model tendencies in the EMAC model shows that the moistening in the Pacific lower stratosphere in control EMAC is the net effect of the interplay of advection of moist tropospheric air masses and dehydration by cloud processes (Supplement Fig. S2). In the region of the moist bias over the Pacific, advective moistening dominates and causes a net moist bias there during boreal summer. Hence, the excessive moisture transport in the standard EMAC model transport scheme appears related to excessive numerical diffusion in the advective transport.

5.1.3 ERA5 reanalysis

The ERA5 reanalysis from the European Centre for Medium-Range Weather Forecasts (ECMWF) covers the period from 1949 onwards (Hersbach et al., 2020). Here, we use monthly mean climatologies compiled from ERA5 wind, PV, geopotential height and temperature data for the period 2005–2015, for better comparability with MLS observations and the climate model simulations. The ERA5 data assimilation system is based on the ECMWF Integrated Forecast System, cycle CY41R2, and uses a 4D-Var assimilation scheme. ERA5 data is available hourly, with a horizontal resolution of about 30 km (T639 spectral resolution), and a vertical range from the surface to about 0.01 hPa (137 hybrid levels). For the monthly mean climatologies shown in this paper we used ERA5 data every 6 hours, truncated to a $1^\circ \times 1^\circ$ latitude-longitude grid and with full vertical resolution, as provided by ECMWF.

5.1.4 CMIP6 model intercomparison project

To place the EMAC simulations into context, we compare to climate model simulations from the Coupled Model Intercomparison Project, Phase 6 (CMIP6). CMIP6 is a multi-model intercompison activity which has been carried out in support of the Sixth Assessment of the IPCC (AR6). Here, we consider the historical simulations which are fully coupled model simulations, with external forcings from solar variability, volcanic aerosols, and anthropogenic emissions (greenhouse gases, aerosol) following observations. If ozone chemistry is not included, the models use prescribed time-varying ozone concentrations. These simulations cover the period 1850–2014, but we only use the data for 2000–2014 for better comparability with the other data sets. From the CMIP6 models investigated recently by Keeble et al. (2021) and which have been shown to have reasonable stratospheric water vapor, those 18 models with the necessary data for this study are: AWI-ESM-1-1-LR, BCC-CSM2-MR, BCC-ESM1, CESM2, CESM2-FV2, CESM2-WACCM, CESM2-WACCM-FV2, CNRM-CM6-1, CNRM-ESM2-1, E3SM-1-1, GFDL-CM4, IPSL-CM6A-LR, MPI-ESM-1-2-HAM, MPI-ESM1-2-HR, MPI-ESM1-2-LR, MRI-ESM2-0, NorESM2-MM, SAM0-UNICON (for further details on the water vapour in these models see Keeble et al., 2021).

https://doi.org/10.5194/egusphere-2023-2196
Preprint. Discussion started: 13 October 2023
© Author(s) 2023. CC BY 4.0 License.

5.1.5 Inter-model correlations

The circulation response to increased stratospheric water vapour above the Pacific in CMIP6 models is analyzed statistically by using inter-model correlations. For that purpose, a Pacific H_2O index is defined by averaging lowermost stratospheric water vapour in the Pacific region (140–220°E longitude, 20–45°N latitude, 150–70 hPa pressure) in each model. This index measures the strength of the Pacific moisture anomaly in different climate models and is correlated with circulation variables (zonal and meridional wind) across models. Hence, a negative correlation with meridional v-wind in the lower stratosphere above the Pacific (about 100–160°E) in Fig. 3, for instance, means that those models with higher water vapour mixing ratios in the Pacific UTLS simulate more negative, equatorward meridional wind in this region. Consequently, the eastern, equatorward flank of the monsoon anticyclonic circulation is strengthened in these models. Similar inter-model correlations have been used for analyzing the westerly ducts in Fig. 3.

5.1.6 Dynamical balances

The large-scale effects on atmospheric circulation from changes in stratospheric water vapour can be understood from simplified, balanced dynamics (Charlesworth et al., 2023), taking into account the radiative effect of water vapour on atmospheric temperatures. An increase of water vapour in the lowermost stratosphere causes local long-wave cooling and thereby modifies the atmospheric temperature gradients in that region. These changes in meridional and zonal temperature gradients $\Delta\left(\partial_y T\right)$ and $\Delta\left(\partial_x T\right)$ are related via the thermal wind relation to changes in u and v–wind velocities

$$\partial_z(\Delta u) = -\frac{R}{H\,f}\Delta\left(\partial_y T\right)\,, \qquad \partial_z(\Delta v) = \frac{R}{H\,f}\Delta\left(\partial_x T\right)\,. \tag{1}$$

For instance, the decrease in the meridional temperature gradient below about 90 hPa above the Pacific (around 200°E) in Fig. 3b is related to an increase in the vertical gradient of zonal wind. Likewise, the increase in the meridional temperature gradient above is related to a decrease in the vertical zonal wind gradient. Hence, the increased water vapour in the Pacific lowermost stratosphere causes increased westerlies in that region, and thereby strengthens the Pacific westerly ducts. Similar relations hold between the changes in the zonal temperature gradient and changes in the vertical gradient of meridional wind (see Eq. 1) such that negative meridional v-wind velocities further decrease around and above the tropopause in the Pacific (at about 130°E), implying a strengthened equatorward flow (Fig. 3). Consequently, increased lower stratospheric water vapour above the Pacific is related to a strengthened equatorward flank on the eastern side of the monsoon anticyclone.

5.1.7 Monsoon anticyclone diagnosis

Different diagnostics have been proposed in the literature for assessing strength and extend of the Asian monsoon anticyclone, based on either geopotential height, Montgomery stream function of potential vorticity (Randel and Park, 2006; Ploeger et al., 2015; Santee et al., 2017). Due to data availability for the considered model simulations we here use geopotential height anomaly as a measure for the anticyclonic circulation. In particular, we follow Bergman et al. (2013) and diagnose the center of the anticyclone as the location of maximum geopotential height on the 100 hPa isobaric surface. Longitude profiles at the

https://doi.org/10.5194/egusphere-2023-2196
Preprint. Discussion started: 13 October 2023
© Author(s) 2023. CC BY 4.0 License.

latitude of the anticyclone center are then used to compare the longitudinal extent of the upper level anticyclonic monsoon circulation in different models (Fig. 4).

Code and data availability. The EMAC and EMAC–CLaMS models are available in the Modular Earth Submodel System (MESSy) git database. Detailed information is available at https://messy-interface.org/licence/application. ERA5 reanalysis data are available from the European Centre for Medium-range Weather Forecasts (https://esgf-node.llnl.gov/search/cmip6). The EMAC and EMAC–CLaMS model data used for this paper may be requested from the corresponding author (f.ploeger@fz-juelich.de). CMIP6 model data is publically available at https://esgf-node.llnl.gov/search/cmip6.

Author contributions. FP initiated the study, carried out the analysis and wrote the manuscript. EC set-up and carried out the model simulations and the data processing. TB and PK were strongly involved in several detailed discussions during different phases of the project. All authors contributed to writing the manuscript.

Competing interests. One of the co-authors (RM) is a member of the editorial board of Atmospheric Chemistry and Physics.

Acknowledgements. We thank Nicole Thomas and Patrick Jöckel for support with setting up the model simulations. This study was funded the Deutsche Forschungsgemeinschaft (DFG, German Research Foundation) – TRR 301 – Project-ID 428312742. Finally, we gratefully acknowledge the computing time for the CLaMS simulations which was granted on the supercomputer JURECA at the Jülich Supercomputing Centre (JSC) under the VSR project ID CLAMS–ESM.

https://doi.org/10.5194/egusphere-2023-2196
Preprint. Discussion started: 13 October 2023
© Author(s) 2023. CC BY 4.0 License.

References

Banerjee, A., Chiodo, G., Previdi, M., Ponater, M., Conley, A. J., and Polvani, L. M.: Stratospheric water vapor: an important climate feedback, Clim. Dyn., 53, 1432–0894, https://doi.org/10.1007/s00382-019-04721-4, https://doi.org/10.1007/s00382-019-04721-4, 2019.

Bergman, J. W., Fierli, F., Jensen, E. J., Honomichl, S., and Pan, L. L.: Boundary layer sources for the Asian anticyclone: Regional contributions to a vertical conduit, J. Geophys. Res., 118, 2560–2575, https://doi.org/10.1002/jgrd.50142, 2013.

Brewer, A. W.: Evidence for a world circulation provided by the measurements of helium and water vapour distribution in the stratosphere, Q. J. R. Meteorol. Soc., 75, 351–363, https://doi.org/10.1002/qj.49707532603, 1949.

Charlesworth, E., Ploeger, F., Birner, T., Baikhadzhaev, R., Abalos, M., Abraham, L., Akiyoshi, H., Bekki, S., Dennison, F., Jöckel, P., Keeble, J., Kinnison, D., Morgenstern, O., Plummer, D., Rozanov, E., Strode, S., Zeng, G., and Riese, M.: Stratospheric water vapor affecting atmospheric circulation, Nat. Commun., 14, 3925, https://doi.org/10.1038/s41467-023-39559-2, 2023.

Charlesworth, E. J., Dugstad, A.-K., Fritsch, F., Jöckel, P., and Plöger, F.: Impact of Lagrangian Transport on Lower-Stratospheric Transport Time Scales in a Climate Model, Atmos. Chem. Phys., 20, 15 227–15 245, https://doi.org/10.5194/acp-20-15227-2020, 2020.

Dessler, A., Schoeberl, M., Wang, T., Davis, S., and Rosenlof, K.: Stratospheric water vapor feedback, Proceedings of the National Academy of Sciences, 110, 18 087–18 091, https://doi.org/10.1073/pnas.1310344110, http://www.pnas.org/content/110/45/18087.abstract, 2013.

Dessler, A., Ye, H., Wang, T., Schoeberl, M., Oman, L., Douglass, A., Butler, A., Rosenlof, K., Davis, S., and Portmann, R.: Transport of ice into the stratosphere and the humidification of the stratosphere over the 21st century, Geophys. Res. Lett., 43, 2323–2329, https://doi.org/10.1002/2016GL067991, 2016.

Fueglistaler, S., Bonazzola, M., Haynes, P. H., and Peter, T.: Stratospheric water vapor predicted from the Lagrangian temperature history of air entering the stratosphere in the tropics, J. Geophys. Res., 110, D08107, https://doi.org/10.1029/2004JD005516, 2005.

Garny, H. and Randel, W. J.: Dynamic variability of the Asian monsoon anticyclone observed in potential vorticity and correlations with tracer distributions, J. Geophys. Res., 118, 13 421–13 433, https://doi.org/10.1002/2013JD020908, 2013.

Hersbach, H., Bell, B., Berrisford, P., Hirahara, S., Horànyi, A., Muñoz Sabater, J., Nicolas, J., Peubey, C., Radu, R., Schepers, D., Simmons, A., Soci, C., Abdalla, S., Abellan, X., Balsamo, G., Bechtold, P., Biavati, G., Bidlot, J., Bonavita, M., De Chiara, G., Dahlgren, P., Dee, D., Diamantakis, M., Dragani, R., Flemming, J., Forbes, R., Fuentes, M., Geer, A., Haimberger, L., Healy, S., Hogan, R. J., Hólm, E., Janisková, M., Keeley, S., Laloyaux, P., Lopez, P., Lupu, C., Radnoti, G., de Rosnay, P., Rozum, I., Vamborg, F., Villaume, S., and Thépaut, J.-N.: The ERA5 global reanalysis, Q. J. R. Meteorol. Soc., 146, 1999–2049, https://doi.org/10.1002/qj.3803, 2020.

Hoor, P., Wernli, H., Hegglin, M. I., and Boenisch, H.: Transport timescales and tracer properties in the extratropical UTLS, Atmos. Chem. Phys., 10, 7929–7944, https://doi.org/10.5194/acp-10-7929-2010, 2010.

Hoppe, C. M., Hoffmann, L., Konopka, P., Grooß, J.-U., Ploeger, F., Günther, G., Jöckel, P., and Müller, R.: The implementation of the CLaMS Lagrangian transport core into the chemistry climate model EMAC 2.40.1: application on age of air and transport of long-lived trace species, Geosci. Model Dev., 7, 2639–2651, https://doi.org/10.5194/gmd-7-2639-2014, http://www.geosci-model-dev.net/7/2639/2014/, 2014.

James, R., Bonazzola, M., Legras, B., Surbled, K., and Fueglistaler, S.: Water vapor transport and dehydration above convective outflow during Asian monsoon, Geophys. Res. Lett., 35, L20810, https://doi.org/10.1029/2008GL035441, 2008.

Jöckel, P., Tost, H., Pozzer, A., Kunze, M., Kirner, O., Brenninkmeijer, C., Brinkop, S., Duy, S. C., Dyroff, C., Eckstein, J., Frank, F., Garny, H., Gottschaldt, K.-D., Graf, P., Grewe, V., Kerkweg, A., Kern, B., Matthes, S., Mertens, A., Meul, S., Neumaier, M., Nützel, M.,

https://doi.org/10.5194/egusphere-2023-2196
Preprint. Discussion started: 13 October 2023
© Author(s) 2023. CC BY 4.0 License.

Oberländer-Hayn, S., Ruhnke, R., Runde, T., Sander, R., Scharffe, D., and Zahn, A.: Earth System integrated Modelling (ESCiMo) with the Modular Earth Submodel System (MESSy) version 2.51, Geosci. Model Dev., 9, 1153–1200, 2016.

Keeble, J., Hassler, B., Banerjee, A., Checa-Garcia, R., Chiodo, G., Davis, S., Eyring, V., Griffiths, P. T., Morgenstern, O., Nowack, P., Zeng, G., Zhang, J., Bodeker, G., Burrows, S., Cameron-Smith, P., Cugnet, D., Danek, C., Deushi, M., Horowitz, L. W., Kubin, A., Li, L., Lohmann, G., Michou, M., Mills, M. J., Nabat, P., Olivié, D., Park, S., Seland, Ø., Stoll, J., Wieners, K.-H., and Wu, T.: Evaluating stratospheric ozone and water vapour changes in CMIP6 models from 1850 to 2100, Atmos. Chem. Phys., 21, 5015–5061, https://doi.org/10.5194/acp-21-5015-2021, https://acp.copernicus.org/articles/21/5015/2021/, 2021.

Konopka, P., Tao, M., Ploeger, F., Hurst, D. F., Santee, M. L., Wright, J. S., and Riese, M.: Stratospheric Moistening After 2000, Geophys. Res. Lett., 49, e2021GL097 609, https://doi.org/https://doi.org/10.1029/2021GL097609, https://agupubs.onlinelibrary.wiley.com/doi/abs/10.1029/2021GL097609, 2022.

Legras, B. and Bucci, S.: Confinement of air in the Asian monsoon anticyclone and pathways of convective air to the stratosphere during the summer season, Atmos. Chem. Phys., 20, 11 045–11 064, https://doi.org/10.5194/acp-20-11045-2020, https://acp.copernicus.org/articles/20/11045/2020/, 2020.

Li, F. and Newman, P.: Stratospheric water vapor feedback and its climate impacts in the coupled atmosphere-ocean Goddard Earth Observing System Chemistry-Climate Model, Clim. Dyn., 55, 1585–1595, https://doi.org/10.1007/s00382-020-05348-6, https://ui.adsabs.harvard.edu/abs/2020ClDy...55.1585L, 2020.

Nützel, M., Podglajen, A., Garny, H., and Ploeger, F.: Quantification of water vapour transport from the Asian monsoon to the stratosphere, Atmos. Chem. Phys., 19, 8947–8966, https://doi.org/10.5194/acp-19-8947-2019, https://www.atmos-chem-phys.net/19/8947/2019/, 2019.

Park, M., Randel, W. J., Emmons, L. K., and Livesey, N. J.: Transport pathways of carbon monoxide in the Asian summer monsoon diagnosed from Model of Ozone and Related Tracers (MOZART), J. Geophys. Res., 114, D08303, https://doi.org/10.1029/2008JD010621, 2009.

Plaza, N. P., Podglajen, A., Peña Ortiz, C., and Ploeger, F.: Processes influencing lower stratospheric water vapour in monsoon anticyclones: insights from Lagrangian modelling, Atmos. Chem. Phys., 21, 9585–9607, https://doi.org/10.5194/acp-21-9585-2021, https://acp.copernicus.org/articles/21/9585/2021/, 2021.

Ploeger, F., Günther, G., Konopka, P., Fueglistaler, S., Müller, R., Hoppe, C., Kunz, A., Spang, R., Grooß, J.-U., and Riese, M.: Horizontal water vapor transport in the lower stratosphere from subtropics to high latitudes during boreal summer, J. Geophys. Res., 118, 8111–8127, https://doi.org/10.1002/jgrd.50636, 2013.

Ploeger, F., Gottschling, C., Grießbach, S., Grooß, J.-U., Günther, G., Konopka, P., Müller, R., Riese, M., Stroh, F., Tao, M., Ungermann, J., Vogel, B., and von Hobe, M.: A potential vorticity-based determination of the transport barrier in the Asian summer monsoon anticyclone, Atmos. Chem. Phys., 15, 13 145–13 159, https://doi.org/10.5194/acp-15-13145-2015, 2015.

Randel, W. J. and Park, M.: Deep convective influence on the Asian summer monsoon anticyclone and associated tracer variability observed with Atmospheric Infrared Sounder (AIRS), J. Geophys. Res., 111, D12314, https://doi.org/10.1029/2005JD006490, 2006.

Read, W. G., Lambert, A., Bacmeister, J., Cofield, R. E., Christensen, L. E., Cuddy, D. T., Daffer, W. H., Drouin, B. J., Fetzer, E., Froidevaux, L., Fuller, R., Herman, R., Jarnot, R. F., Jiang, J. H., Jiang, Y., Kelly, K., Knosp, B. W., J.Kovalenko, L., Livesey, N. J., Liu, H.-C., Manney, G. L., Pickett, H. M., Pumphrey, H. C., Rosenlof, K. H., Sabounchi, X., Santee, M. L., Schwartz, M. J., Snyder, W. V., Stek, P., Su, H., Takacs, L. L., Thurstans, R. P., Voemel, H., Wagner, P. A., Waters, J. W., Webster, C. R., Weinstock, E. M., and Wu, D. L.: Aura Microwave Limb Sounder upper tropospheric and lower stratospheric H_2O and relative humidity with respect to ice validation, J. Geophys. Res., 112, D24S35, https://doi.org/10.1029/2007JD008752, 2007.

https://doi.org/10.5194/egusphere-2023-2196
Preprint. Discussion started: 13 October 2023
© Author(s) 2023. CC BY 4.0 License.

Rolf, C., Vogel, B., Hoor, P., Afchine, A., Günther, G., Krämer, M., Müller, R., Müller, S., Spelten, N., and Riese, M.: Water vapor increase in the lower stratosphere of the Northern Hemisphere due to the Asian monsoon anticyclone observed during the TACTS/ESMVal campaigns, Atmospheric Chemistry and Physics, 18, 2973–2983, https://doi.org/10.5194/acp-18-2973-2018, https://www.atmos-chem-phys.net/18/2973/2018/, 2018.

Santee, M. L., Manney, G. L., Livesey, N. J., Schwartz, M. J., Neu, J. L., and Read, W. G.: A comprehensive overview of the climatological composition of the Asian summer monsoon anticyclone based on 10 years of Aura Microwave Limb Sounder measurements, J. Geophys. Res., 122, 5491–5514, https://doi.org/10.1002/2016JD026408, https://agupubs.onlinelibrary.wiley.com/doi/abs/10.1002/2016JD026408, 2017.

Schoeberl, M. R., Dessler, A. E., and Wang, T.: Modeling upper tropospheric and lower stratospheric water vapor anomalies, Atmos. Chem. Phys., 13, 7783–7793, https://doi.org/10.5194/acp-13-7783-2013, 2013.

Smith, J. W., Bushell, A. C., Butchart, N., Haynes, P. H., and Maycock, A. C.: The Effect of Convective Injection of Ice on Stratospheric Water Vapor in a Changing Climate, Geophys. Res. Lett., 49, e2021GL097 386, https://doi.org/10.1029/2021GL097386, 2022.

Solomon, S., Rosenlof, K., Portmann, R., Daniel, J., Davis, S., Sanford, T., and Plattner, G.-K.: Contributions of stratospheric water vapor to decadal changes in the rate of global warming, Science, 327, 1219–1223, https://doi.org/10.1126/science.1182488, 2010.

Stenke, A., Dameris, M., Grewe, V., and Garny, H.: Implications of Lagrangian transport for simulations with a coupled chemistry-climate model, Atmos. Chem. Phys., 9, 5489–5504, http://www.atmos-chem-phys.net/9/5489/2009/, 2009.

von Hobe, M., Ploeger, F., Konopka, P., Kloss, C., Ulanowski, A., Yushkov, V., Ravegnani, F., Volk, C. M., Pan, L. L., Honomichl, S. B., Tilmes, S., Kinnison, D. E., Garcia, R. R., and Wright, J. S.: Upward transport into and within the Asian monsoon anticyclone as inferred from StratoClim trace gas observations, Atmos. Chem. Phys., 21, 1267–1285, https://doi.org/10.5194/acp-21-1267-2021, https://acp.copernicus.org/articles/21/1267/2021/, 2021.

Wang, X., Wu, Y., Tung, W., Richter, J. H., Glanville, A. A., Tilmes, S., Orbe, C., Huang, Y., Xia, Y., and Kinnison, D. E.: The Simulation of Stratospheric Water Vapor Over the Asian Summer Monsoon in CESM1(WACCM) Models, J. Geophys. Res., 123, 11 377–11 391, https://doi.org/10.1029/2018JD028971, 2018.

Waugh, D. W. and Polvani, L. M.: Climatology of intrusions into the tropical upper troposphere, Geophys. Res. Lett., 27, 3857–3860, 2000.

Webster, P. J. and Holton, J. R.: Cross-equatorial response to middle-latitude forcing in a zonally varying basic state, jas, 39, 722–733, 1982.

Wright, J. S., Fu, R., Fueglistaler, S., Liu, Y. S., and Zhang, Y.: The influence of summertime convection over Southeast Asia on water vapor in the tropical stratosphere, J. Geophys. Res., 116, D12302, https://doi.org/10.1029/2010JD015416, 2011.

Yan, X., Konopka, P., Hauck, M., Podglajen, A., and Ploeger, F.: Asymmetry and pathways of inter-hemispheric transport in the upper troposphere and lower stratosphere, Atmos. Chem. Phys., 21, 6627–6645, https://doi.org/10.5194/acp-21-6627-2021, 2021.